Analysis of the Dynamics of a Slider-Crank Mechanism Locally Actuated with an Act-And-Wait Controller

Jarl Beckers[a,b,*], Tom Verstraten[c], Bjorn Verrelst[c], Francesco Contino[d], Joeri Van Mierlo[b,e]

[a] *Thermo and Fluid dynamics (FLOW) Faculty of Engineering, Vrije Universiteit Brussel (VUB) Pleinlaan 2, 1050 Brussels, Belgium.*
Email: jarl.beckers@vub.be
[b] *Mobility Logistic and Automotive Technology Research Group (MOBI), Department of Electrical Engineering and Energy Technology (ETEC), Vrije Universiteit Brussel, Pleinlaan 2, 1050 Brussels, Belgium.*
[c] *Robotics & Multibody Mechanics Research Group (R&MM), Faculty of Mechanical Engineering, Vrije Universiteit Brussel, Brussels, 1050, Belgium.*
[d] *Institute of Mechanics, Materials and Civil Engineering (iMMC), Université catholique de Louvain (UCLouvain), Place du Levant, 2, 1348 Louvain-la-Neuve, Belgium*
[e] *Flanders Make, 3001 Heverlee, Belgium.*

Abstract

Traditional use of slider-crank mechanisms result in high loads transmitted through the mechanical structure, inhibiting the design of a compact machine. Therefore, this paper proposes to step away from the conventional, i.e. rotative, actuation and to investigate local linear actuation of the slider-component directly, while maintaining the kinematic link. In this work the equation of motion and corresponding non-isochronous movement are derived for the proposed system, loaded with a linear spring-damper element. This knowledge is afterwards incorporated in an act-and-wait control strategy, implemented in a multibody model in *Simscape*, to evaluate the local linear actuating principle. The obtained configuration results both in a continuous movement of the slider mechanism where Top Dead Centre & Bottom Dead Centre are reached and in a minimisation of the loads transmitted through the mechanical structure. Further investigation of one of the most determining parameters, i.e. the operating frequency, proves that operating at the resonance frequency of the system, yields optimal results. This configuration

*Corresponding Author

allows for the reduction of the loads transmitted through the system by 90% of the nominal spring-damper load.

Keywords: Slider-Crank Mechanism, Lagrange Equations, Resonance, Act-And-Wait, Non-isochronous

---

Nomenclature

BDC	Bottom dead centre
C	Damping coefficient $[Ns/m]$
F	Force $[N]$
g	Gravitational acceleration constant $[N/kg]$
I	Moment of inertia $[kg\ m^2]$
k	Spring stiffness $[N/m]$
l	Length connecting rod $[m]$
m	Mass $[kg]$
r	Length crank rod $[m]$
ref	Reference
TDC	Top dead centre
x	Position $[m]$
Δ	Finite difference
θ	Crank angle $[^\circ]$
ϕ	Connecting rod angle $[^\circ]$

Subscripts

0	Initial
act	Actuation
$crit$	Critical
eq	Equivalent
l	Connecting rod
max	Maximum
os	Oscillation
p	Piston
r	Crank
s	Static

1. Introduction

In industrial applications such as diesel and gasoline engines or piston compressors and pumps, a slider-crank mechanism is used to convert a rotary motion into a linear motion or vice-versa. The resulting technology and associated mechanical structure have been investigated extensively in the past decades [1]. However, in such applications, the kinematic structure is dimensioned to transmit the full power from piston to motor side and

vice versa. As a result, journal bearings are often used to cope with the high loads transmitted through the system, complicating the possibility of a compact and hermetic solution [2, 3]. Recent research focuses furthermore on the dynamic analysis of such a system, taking into account the relative motion in and loads acting on these joints. Daniali et al. performed such a dynamic investigation including the clearances in the joints and proposed an optimisation of the mass distribution of the links of a mechanism to reduce or eliminate the impact forces in the clearance joint [4]. Yaqubi et al. investigated the possibility of improving performance by using clearance control in joints accompanied with a second actuator on the connecting rod to reduce the vibrations and load on the first actuator [5]. Hong-Sen Ya proposes the use of a stepper motor to step away from the traditional trajectories associated to a constant speed input. By properly designing the input speed of the mechanism, the output motion can pass through a desired trajectory [6]. A similar strategy has been adopted in [7] and [8] for a 4-bar mechanism. As a result, further research focuses on adequate actuation and (torque) control strategies to obtain a desired output profile [9, 10, 11]. Other possibilities have been investigated extensively such as the use of adjustable slider-crank mechanisms to obtain atypical trajectories [12, 13, 14]. An alternative configuration has been demonstrated by Sarigecili where a constant output force on the slider is obtained, independent of the crank angle, by adding a second (controlled) input force on the crank–connecting rod joint [15]. Soong goes a step further and details the design of flexible linkage mechanisms with a rotational input and a linear input combined [16] and similarly in [17] where such an innovative configuration is presented in a hybrid-driven mechanical press. As a result, we propose to investigate in depth the possibilities (and associated dynamics) of local (linear) actuation on the linear component of a slider-crank mechanism, i.e. slider, without rotational input. This means that the full power is provided to the linear component directly to counteract the loads, rather than provided rotationally and fully transmitted through the mechanical system. Such configuration would allow to minimise the loads in the joints and reduce the power transmitted through the system significantly, compared to previous research [6, 16, 17]. This allows to downsize the mechanical structure and the entire machine in general. Furthermore, it would still provide the opportunity to impose any desired trajectory (and associated control strategies), be it with mechanical limits. Maintaining this mechanical link, provides a fail safe if an excessive force is imposed on the slider-component, which would allow to simplify control strategies compared

to e.g. free piston compressors [18]. Therefore, to evaluate the proposed local actuation, a simple act-and-wait control strategy (denoted as bang-bang-control) on a slider-crank system with generic load, i.e. mechanical spring, is investigated. The focus of this control strategy lies on minimising the forces or loads transmitted through the mechanical structure while guaranteeing that top & bottom dead centre (TDC & BDC) are reached.

To fully investigate the possibilities and to clarify the optimal working conditions, this paper starts by detailing the dynamics and natural motion of an unforced slider-crank system loaded with a spring-damper element in Section 2.1. Afterwards, the developed multibody simulation environment in *Simscape* and the proposed bang-bang control strategy are detailed in Section 2.2. To conclude, the obtained simulation results are discussed in Section 3 and the optimal steady state working conditions (minimal load in the mechanical structure) are presented as a result of such a system configuration, i.e. at its resonance frequency. A quick comparison with the analytical results is provided to justify the obtained numerical results.

2. Simulation model

In a first step, a dynamic analysis of a slider-crank mechanism loaded with a spring-damper element is detailed to investigate the non-isochronous movement of the system. The geometry illustrated in Fig. 1a, where F_{act} represents the local actuation force on the slider. Afterwards, a numerical approach has been adopted using *Simscape Multibody* to evaluate the performance of the local actuation on the piston. The system displayed in Fig. 1a has been implemented in the multibody environment and the resulting lay-out is presented in Fig. 1b.

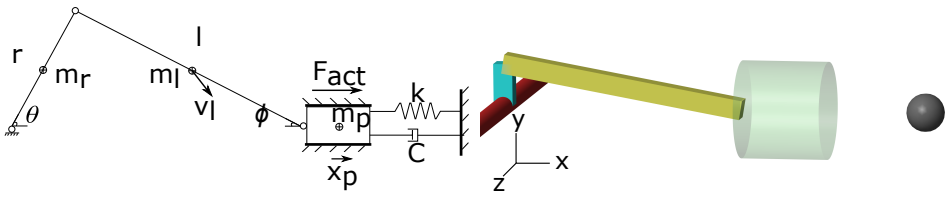

(a) Schematic drawing of a slider-crank mechanism attached to a translational spring-damper element.

(b) Simscape lay-out of a slider-crank mechanism loaded with a mechanical spring-damper element.

Figure 1: Slider-crank mechanism.

The model consists of a shaft (indicated in red in Fig. 1b) connected to the ground with a revolute joint, a crank rod (indicated in blue) rigidly connected to the shaft, a connecting rod (indicated in yellow) connected to the crank rod and piston with 2 revolute joints and a piston (indicated in transparent green) whose motion is limited using a translational joint w.r.t. the ground. The spring-damper element has been implemented as a linear force acting between the piston and ground, visualised by the "dummy" grey ball. The system has its resting position at half of the stroke. The numerical configuration considered throughout this paper is listed in Table 1. The spring stiffness and damping coefficient have been chosen based on the specifications of an available test set-up to be within its nominal operating conditions. This allows for a straightforward comparison of the obtained simulation results in this paper with future experiments.

Table 1: Specifications of the slider-crank mechanism analysis.

Length crank rod r (mm)	22.1
Length connecting rod l (mm)	127
Mechanical stiffness spring k (N/m)	760
Mechanical damping coefficient damper C (Ns/m)	1
Natural length spring at half the stroke l_0 (mm)	50
Maximum static spring force $F_{s,max}$ (N)	16.8
Mass crank rod m_r (kg)	0.017
Mass connecting rod m_l (kg)	0.099
Mass piston m_p (kg)	0.72
Polar inertia crank rod I_r(kg mm^2)	2.94
Polar inertia connecting rod I_l (kg mm^2)	533

2.1. Dynamic analysis of a slider-crank mechanism

To obtain an initial understanding of the dynamic behaviour of a slider-crank mechanism loaded with a spring, the equations of motion can be established using Fig. 1a. The following kinetic energy (T) and potential energy (V) formulations can be derived. Assuming a uniform material distribution and reflecting the inertias to the revolute joints using the parallel axis theorem, the kinetic energy of the system can be written as the combination of the linear movement of piston and connecting rod, together with the rotation

of the crank rod and tilting of the connecting rod.

$$\begin{aligned} T &= \frac{1}{2} I_r \dot{\theta}^2 + \frac{1}{2} I_l \dot{\phi}^2 + \frac{1}{2} m_l v_l^2 + \frac{1}{2} m_p v_p^2 \\ V &= m_r g \frac{r}{2} sin(\theta) + m_l g \frac{l}{2} sin(\phi) + \frac{k}{2} \Delta x^2 \end{aligned} \tag{1}$$

With

- $v_l = \sqrt{(r\sin\theta + \frac{r^2 \sin\theta\cos\theta}{2\sqrt{l^2 - r^2\sin^2\theta}})^2 + (\frac{r}{2}\cos\theta)^2}\dot{\theta}$
- $\dot{\phi} = \frac{r\cos\theta}{l\sqrt{1-(\frac{r}{l}\sin\theta)^2}}\dot{\theta}$
- $v_p = (-r\sin\theta - \frac{r^2\sin\theta\cos\theta}{\sqrt{l^2 - r^2\sin^2\theta}})\dot{\theta}$
- $\Delta x = r\cos\theta + \sqrt{l^2 - r^2\sin^2\theta} - l$

Writing down the Lagrangian and performing the required derivations, yield the following equation of motion Eq. 2 describing the unforced movement of a slider-crank mechanism loaded with a spring-damper mechanism. For the interested reader, the full derivation is detailed in Appendix A.

$$\begin{aligned} & I_r\ \ddot{\theta} + I_l \frac{r^2\cos^2\theta}{a^2}\ddot{\theta} + m_p \left(r\sin\theta + \frac{r^2\sin\theta\cos\theta}{a} \right)^2 \ddot{\theta} \\ & \quad + m_l \left(\left(r\sin\theta + \frac{\frac{1}{2}r^2\sin\theta\cos\theta}{a} \right)^2 + \left(\frac{r}{2}\cos\theta \right)^2 \right) \ddot{\theta} + I_l \dot{\theta}^2 \frac{r\cos\theta}{a} \frac{-r\sin\theta a - \frac{da}{d\theta} r\cos\theta}{a^2} \\ & \quad + m_p \dot{\theta}^2 \left(r\sin\theta + \frac{r^2\sin\theta\cos\theta}{a} \right) \left(r\cos\theta + \frac{r^2\left(\cos^2\theta - \sin^2\theta\right)a - \frac{da}{d\theta} r^2\sin\theta\cos\theta}{a^2} \right) \\ & \quad + m_l \dot{\theta}^2 \left(r\sin\theta + \frac{\frac{r^2}{2}\sin\theta\cos\theta}{a} \right) \left(r\cos\theta + \frac{1}{2}\frac{r^2\left(\cos^2\theta - \sin^2\theta\right)a - \frac{da}{d\theta} r^2\sin\theta\cos\theta}{a^2} \right) \\ & \quad - m_l \dot{\theta}^2 \left(\frac{r}{2}\cos\theta \right) \frac{r}{2}\sin\theta + (m_r + m_l) g \frac{r}{2}\ \cos\theta + k\ \left(r\cos\theta + a\ - l \right) \left(-r\sin\theta + \frac{da}{d\theta} \right) \\ & \quad =\ -C\ (-r\sin\theta - \frac{r^2\sin\theta\cos\theta}{\sqrt{l^2 - r^2\sin^2\theta}})^2\dot{\theta} \end{aligned} \tag{2}$$

With:

$$\begin{aligned} a &= \sqrt{l^2 - r^2 \sin^2 \theta} \\ \frac{da}{d\theta} &= -\frac{r^2 \sin\theta \cos\theta}{a} \end{aligned} \tag{3}$$

Having established this equation, provides the opportunity to study the unforced natural motion of the slider-crank mechanism highlighted in Fig. 1a. Fig. 2 displays the evolution of the crank angle of the system, defined in Table 1, for different initial angles (denoted as θ_0), obtained by solving Eq. 2 numerically in *Matlab*. No actuation forces are considered on the slider in this experiment. Fig. 2 proves that the larger the oscillation is (the closer θ_0 to 0° or 180°), the larger the oscillation period and thus the lower the frequency. A non-isochronous movement similar to an oscillating pendulum can be noticed, where the oscillating frequency depends on the release angle [19]. The oscillation dampens out to $\theta \approx 85°$, corresponding to the middle of the stroke and the resting position of the spring.

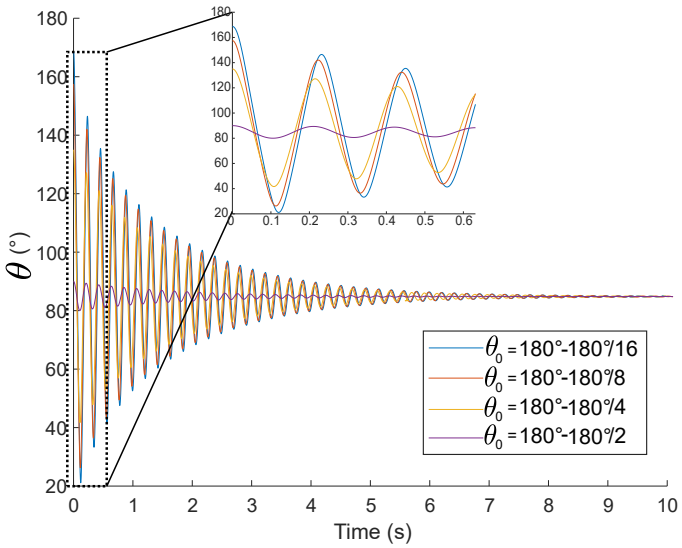

Figure 2: Evolution of the crank angle θ for different starting angles θ_0 without external forces acting on the system.

To conclude the analytical part of this paper, a theoretical derivation of the oscillating frequency as a function of the oscillation amplitude is provided. Assuming that the system is at rest at angle θ_0 upon starting, the following

equation Eq. 4 can be obtained, starting from the energy equations in Eq. 1 and using the conservation of energy theorem, with $a_0 = \sqrt{l^2 - r^2 \sin^2\theta_0}$:

$$\begin{aligned}\frac{1}{2}I_r\ \dot{\theta}^2 + \ \frac{1}{2}I_l\frac{r^2\cos^2\theta}{a^2}\dot{\theta}^2 + \frac{1}{2}m_p\left(-r\sin\theta - \frac{r^2\sin\theta\cos\theta}{a}\right)^2\dot{\theta}^2 \\ + \frac{1}{2}m_l\left(\left(r\sin\theta + \frac{\frac{1}{2}r^2\sin\theta\cos\theta}{a}\right)^2 + \left(\frac{r}{2}\cos\theta\right)^2\right)\dot{\theta}^2 \\ = \ (m_r + m_l)g\frac{r}{2}\sin\theta_0 + \frac{k}{2}\ (r\cos\theta_0 + a_0\ - l)^2 - (m_r + m_l)g\frac{r}{2}\sin\theta - \frac{k}{2}\ (r\cos\theta + a\ - l)^2\end{aligned} \tag{4}$$

Isolating $\dot{\theta}$ and integrating over 1 cycle θ_{cycle} yields the oscillation period T_{os} as function of the starting angle θ_0:

$$T_{os}\ = \int_{\theta_{os}}\ \sqrt{\frac{I_r\ +\ I_l\frac{r^2\cos^2\theta}{a^2} + m_p\left(-r\sin\theta - \frac{r^2\sin\theta\cos\theta}{a}\right)^2 + m_l\left(\left(r\sin\theta + \frac{\frac{1}{2}r^2\sin\theta\cos\theta}{a}\right)^2 + \left(\frac{r}{2}\cos\theta\right)^2\right)}{\frac{1}{2}\left((m_r + m_l)g\frac{r}{2}\sin\theta_0 + \frac{k}{2}(r\cos\theta_0 + a_0 - l)^2 - (m_r + m_l)g\frac{r}{2}\sin\theta - \frac{k}{2}(r\cos\theta + a - l)^2\right)}}\ d\theta \tag{5}$$

Having obtained the oscillation period as a function of the oscillation amplitude, provides the opportunity to quantify the unforced oscillating frequency for the system defined in Fig. 1a and Table 1. The resulting frequency, as a function of the starting angle θ_0 is illustrated in Fig. 3. The closer the initial angle θ_0 is to 0° or 180°, the larger the oscillation amplitude will be and the lower the frequency, in agreement with Fig. 2. Furthermore, the curve is not symmetrical since the resting position of the spring is at half the stroke, i.e. 85°. As a result, a similar behaviour is expected for angles between 180° and 360° crank angle, with a resting position of 275°. In other words, the mass and inertia of the oscillating crank-rod contribute to the natural (linear) motion of the slider and connecting rod. The larger the oscillation, the bigger the contribution of the crank-rod (and connecting rod) to this motion and the lower the frequency will be. The peaks close to 0 ° and 180° are a consequence of the gravity acting on the crank and connecting rods. Evaluating Eq. 5 with g = 0 m/s^2 yields the orange curve in Fig. 3.

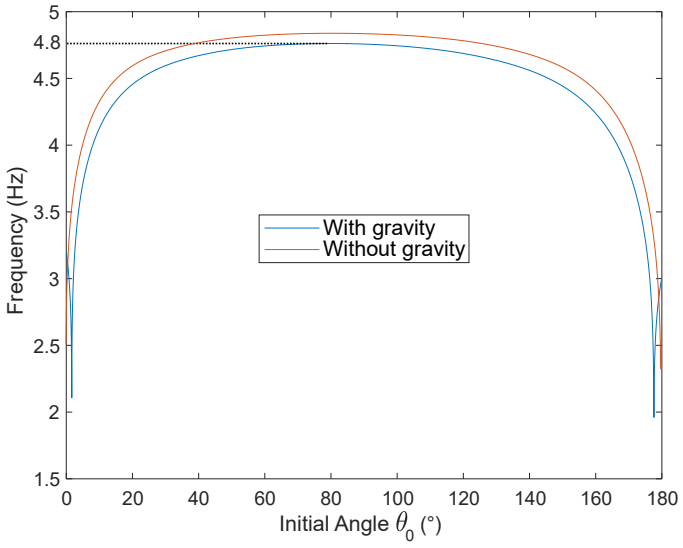

Figure 3: Oscillating frequency as a function of the release angle θ_0.

2.2. Act-and-wait controller

Having explored the non-isochronous movement analytically, the focus shifts towards the investigation of the behaviour of a slider-crank mechanism where the linear motion is imposed to the slider. The idea is to utilise the dynamics of the system by launching the piston, by pushing and pulling it with a linear actuator, instead of controlling it rotationally, similarly to what occurs in combustion engines. In order to do this, the numerical model has been developed in *Simscape Multibody* (Fig. 1b). Using a simple bang-bang controller, rather than complex position controllers [18], over a period of time, the actuation force on the slider will have the shape illustrated in Fig. 4. The goal is hereby to guarantee rotation, by adapting the height of the pulse, such that top & bottom dead centre (TDC & BDC) are reached while minimising the loads in the mechanical structure. These loads are measured in the revolute joint connecting the piston with the connecting rod and are denoted *rod loads*. The maximum rod loads are to be found at the turning points where the mechanical structure absorbs the reaction forces as a result of the large accelerations associated with the speed-reversal of the piston at TDC & BDC. These maxima are used in a traditional feedback loop, where they are compared to a reference rod load that is as low as possible, to adapt the height of the pulse as indicated in Fig. 5. Unfortunately a zero rod load is not achievable as a certain acceleration is required at TDC &

BDC to avoid getting stuck in a singular configuration. Therefore a minimal (non-zero) rod load while rotating is desired. The width of the actuation pulses is fixed throughout this paper, i.e. during 25 % of the oscillation period a positive force is imposed and during 25 % of the oscillation period a negative force is imposed (Fig. 4). During the remaining 50% no actuation force is acting on the system. This means that the frequency of actuation follows the oscillating (and eventually rotating) frequency. More specifically, within 1 cycle, a constant positive force is imposed from BDC to 90° crank angle and a constant negative force from TDC to -90° crank angle. This allows to guarantee that the *launch* parts and *inertial motion* parts of the cycle (Fig. 4) are always at the same axial positions. This simplifies future experiments upon optimally placing a linear actuator to provide the (fixed) range of motion. As a result, the height of the pulse is the only control parameter considered throughout this paper.

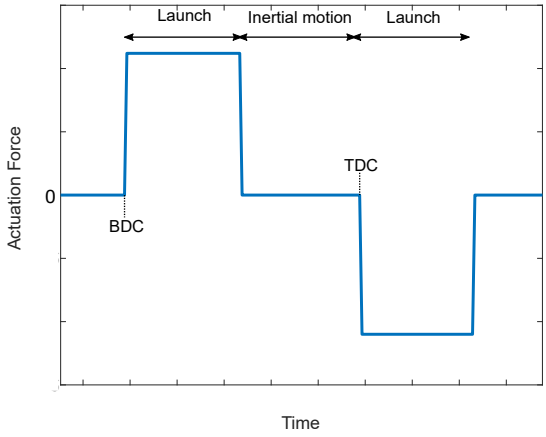

Figure 4: Concept of the bang-bang actuation force profile over 1 time period.

Since a certain minimal acceleration is required at the turning points, the imposed control strategy consists of 2 separate controllers counteracting one another. The position (or transient) controller (loop 1 in Fig. 5) will try to increase the pulse height to guarantee rotation, while the rod load controller (loop 2 in Fig. 5) will try to decrease it to minimise the rod load. The global strategy is illustrated in Fig. 5 and the 2 controllers are detailed in the following sections.

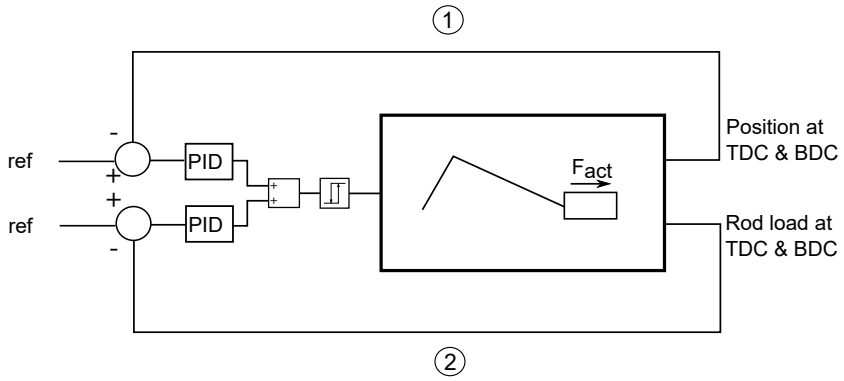

Figure 5: Bang-Bang control strategy consisting of a transient position controller to guarantee rotation and a rod load controller to minimise the loads in the mechanical structure.

The position controller, which allows to start up the system when the mechanical structure is not in a singular configuration, increases systematically the pulse height based on the position error at the oscillating points. In other words, at the end positions of the oscillation, indicated with the yellow and red arrows in Fig 6a, the position of the piston is compared w.r.t. the desired BDC & TDC positions. This allows to determine the respective BDC & TDC-error, in this case x_p (Fig. 1a) with respect to -22.1 mm and +22.1 mm respectively, which determines the pulse height in the next cycle. At this point the crank-rod is oscillating and not yet rotating and as a result the amplitude of the oscillation will increase (the respective TDC & BDC-errors will thus decrease) until at a certain point the shaft starts rotating. The transient result is illustrated in Fig. 6b.

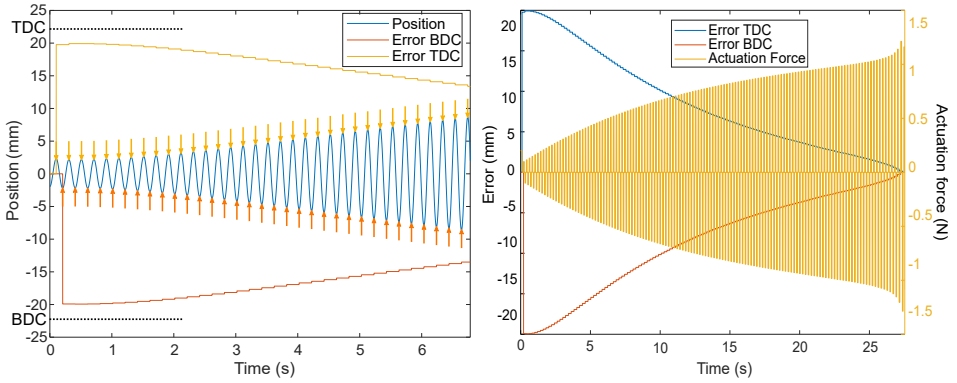

(a) BDC & TDC-errors based on the position of the piston at the oscillating points w.r.t. BDC & TDC position.

(b) Systematic increase of the oscillation amplitude until BDC & TDC are reached and rotation of the crankshaft can be guaranteed.

Figure 6: Position controller results.

The rod load controller however will measure the loads transmitted through the system at the oscillating (during transient) and afterwards the turning points (during steady state) of the cycle and will act accordingly. During the transient, due to the increasing oscillating motion, the rod load increases until rotation is guaranteed (Fig. 7). Therefore, the position controller is set to act as the dominant one (higher control gains) until the crank-rod starts rotating. Afterwards, the rod load controller can and will systematically decrease the rod load, without interference, since the BDC & TDC position errors are zero beyond this point as illustrated in Fig. 8.

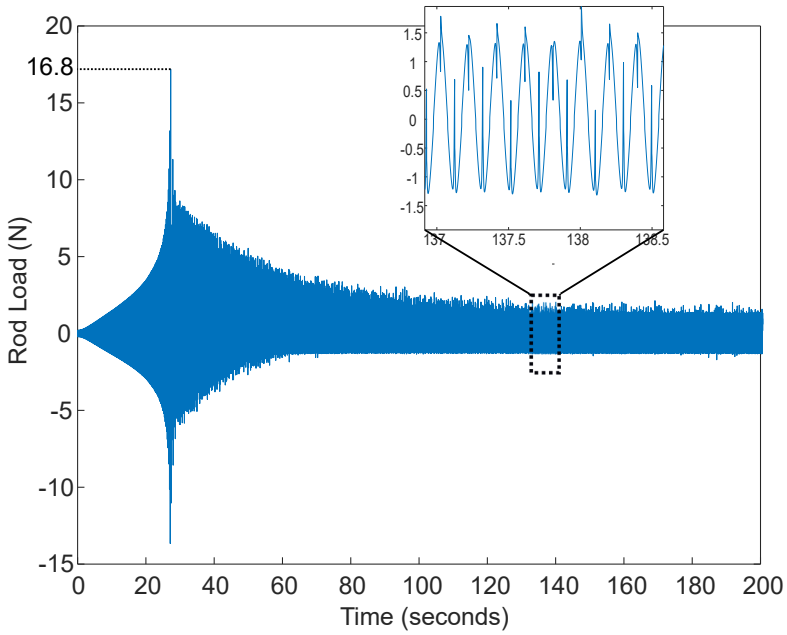

Figure 7: Rod load curve measured in the revolute joint connecting the piston to the connecting rod.

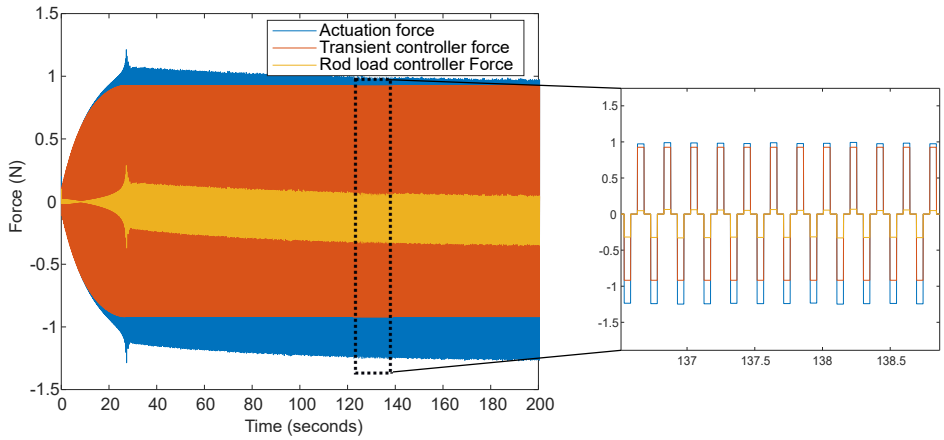

Figure 8: Corresponding actuation force to Fig. 7, where the rod load controller reduces the height of the pulse once rotation is guaranteed.

3. Discussion

When evaluating Fig. 7 and Fig. 8, the actuation force (or height of the force pulse) is increasing at each step during the transient as a result of the position controller. Consequently, the increasing spring forces and inertia forces of the oscillating parts, crank rod, connecting rod and piston, result in an increase of the rod load. At approximately 25 seconds the maximum oscillation amplitude is reached and the crank mechanism starts rotating. After this point, a decrease in the rod load can be observed up to less than 10% of the load acting on the system, i.e. 1.5 N rod load compared to approximately 17 N spring force at the end positions as indicated in Table 1 and in Fig. 7. By systematically decreasing the amplitude of the actuation force, while maintaining a continuous rotation, a minimisation of the rod load is thus feasible. As mentioned before, a zero rod load is not achievable as a certain acceleration, and thus reaction force, is required to avoid getting stuck in the singular configurations at TDC and BDC.

The simulation detailed above proves the feasibility of local actuation to obtain a minimal loading of the mechanical structure once the crank rod is rotating at steady state. A deeper investigation of both the oscillating transient part and the rotating steady state part is provided in the following section and the focus will be on:

- the evolution of the operating frequency during a start-up;
- the relation between the rod load at steady state and the operating frequency.

Let us start by focusing on the latter by performing a series of open loop simulations to evaluate the dependency between the operating frequency and resulting rod load. This allows to quantify the optimal working conditions in terms of minimal load transmitted through the system. Each simulation consists in imposing a fixed actuation pulse height and waiting until rotation is achieved. Afterwards, the frequency and corresponding rod load are determined. A minimal (constant) impulse force of 1.02 N positive and -1.1 N negative is required to guarantee rotation at steady state (cfr. controlled actuation force indicated in Fig. 8 at moment of rotation, i.e. ≈ 27 s), yielding the lowest achievable operating frequency. By systematically increasing this pulse height, the operating/rotating frequency will increase and the following set of results is obtained (Fig. 9).

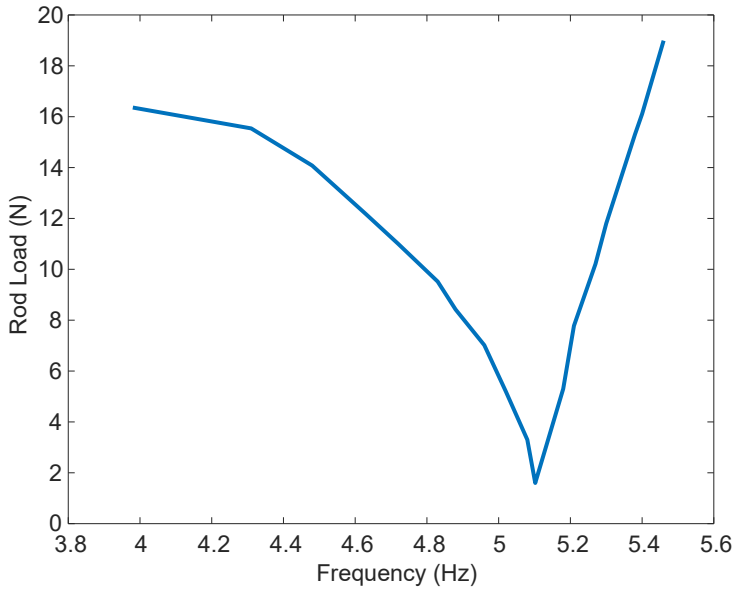

Figure 9: Rod load versus operating frequency upon rotation.

A first (logical) conclusion is that a minimal frequency (here $\approx 4Hz$) is required to guarantee rotation since, as mentioned before, a minimal acceleration is required to obtain a smooth rotation of the crankshaft. Afterwards, the rod load drops the closer the frequency goes to the resonance frequency of the system, approximately equal to:

$$f_{crit,approximated} = \frac{1}{2\pi}\sqrt{\frac{k_{spring}}{m_p + m_l}} = 5.1 \text{ Hz} \tag{6}$$

Once the resonance frequency is crossed, the rod load increases significantly with the frequency as the reaction forces, due to the large accelerations at TDC & BDC, are to be absorbed by the mechanical structure.

The second investigation focuses on the evolution of the operating frequency during transient. Since during the transient, at 1 point the nominal load of 17 N is to be absorbed by the mechanical structure, the question arises if this load can be reduced by carefully tracking the resonance frequency of the system. Evaluating the frequency evolution over time of the simulation results detailed in Fig. 7 and Fig. 8, the following results are obtained:

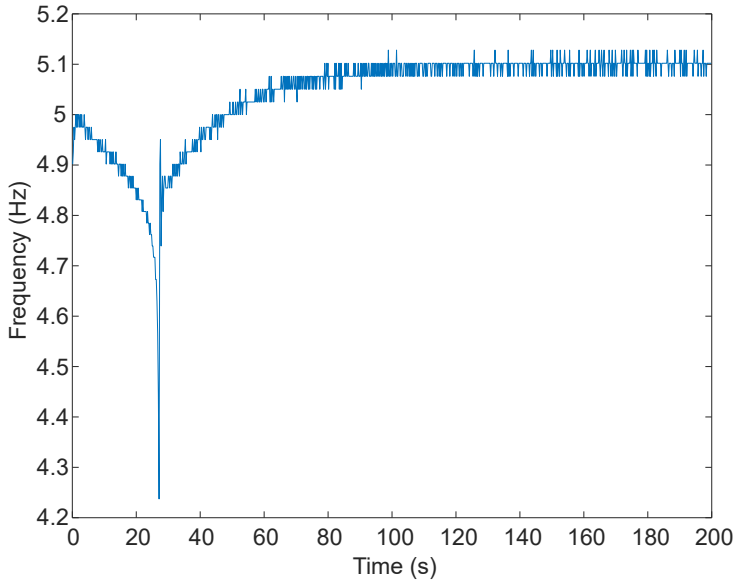

Figure 10: Operating frequency versus time for the simulations detailed in Fig. 7 and Fig. 8.

During start-up, the crank-rod is oscillating and not rotating. As a result the inertia of the oscillating crank-rod contributes to the natural (linear) motion of the slider and connecting rod. The larger the oscillation, the bigger the contribution of the crank-rod (and connecting rod) to this motion and the lower the resonance frequency will be. At around 27 seconds, just before rotation is guaranteed, the maximum oscillation and thus contribution is obtained and as a result, the minimal frequency. Afterwards, when the crankshaft is rotating continuously, the crank-rod will no longer contribute towards the natural motion (as it is no longer oscillating). The resulting resonance frequency will therefore increase again immediately up to ≈ 5 Hz. The further increase in frequency is due to the imperfection of the controller, increasing the velocity to guarantee rotation, while allowing a certain minimal (but not zero) rod load. This frequency evolution can also be quantified by evaluating the increasing equivalent mass of the crank rod. The polar inertia of the crank rod can be reflected to the piston side with an equivalent mass $m_{r,eq}$ using the kinetic energy, with v_p the linear piston velocity:

$$\frac{1}{2} m_{r,eq} v_p^2 = \frac{1}{2} I_r \dot{\theta}^2 \tag{7}$$

Plotting the evolution of this equivalent mass in Fig. 11, proves the reason-

ing behind the decreasing resonance frequency until at around 27 seconds rotation occurs and the equivalent mass is at its maximum. Afterwards, when the crank rod is rotating, the translational velocity v_p is zero at TDC & BDC, while the rotational velocity $\dot{\theta}$ is not, resulting in the fact that eq. 7 goes to infinity.

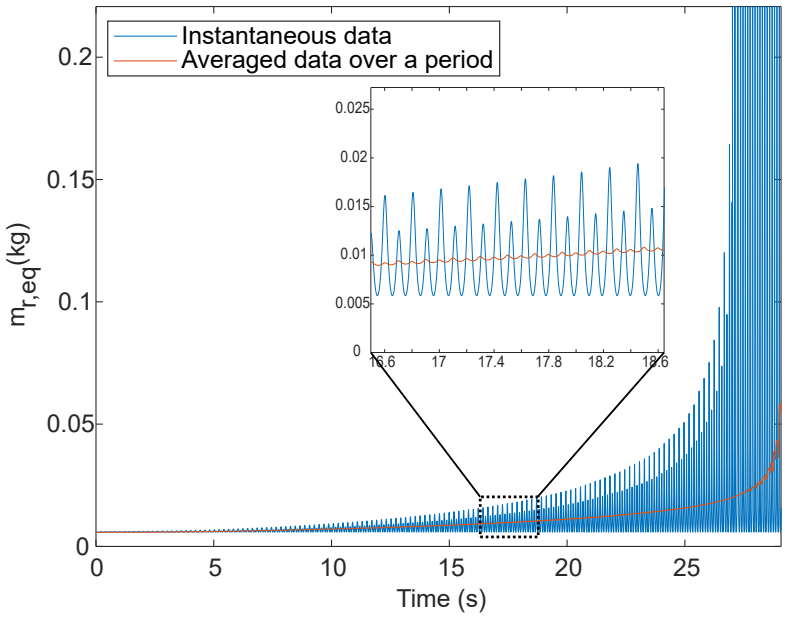

Figure 11: Evolution of the equivalent crank mass upon reflecting the polar inertia of the crank rod to the piston side during transient operation.

Hence, a similar conclusion can be made compared to the analytical analysis section 2.1. The larger the oscillation amplitude, the smaller the operating frequency will be until the crank-rod starts rotating. The discontinuity of the contribution of the crank rod at the point of rotation results in this sudden change of frequency. After this point, we can no longer talk about an non-isochronous oscillating movement of the system, detailed in Fig. 3, and operating/rotating at the resonance frequency, yields the lowest loads transmitted through the mechanical structure.

4. Conclusion

This paper proposed to step away from the traditional use of a slider-crank mechanism by investigating the influence of a local linear actuation

on the slider loaded with a linear spring-damper system. In a first step, a dynamic analysis of this system is provided by establishing the equation of motion and characterising the oscillation-amplitude dependency of the unforced system. On top of that, the derivation of the analytical equation defining the oscillation period as a function of the starting angle is provided, proving the results obtained throughout this paper. Afterwards, the proposed act-and-wait control strategy, i.e. bang bang, has been implemented in a multibody simulation environment with as goal to minimise the forces transmitted through the mechanical structure during steady state operation. A combination of a position and (rod) load controller is introduced, where the subtle counteraction of the 2 controllers results both in a continuous rotation of the crank rod and a minimal rod load in the structure. These loads can be reduced below 10% of the external spring-damper forces acting on the system during steady state conditions. To conclude, the optimal steady state working conditions are presented, i.e. at resonance frequency, as well as an initial investigation of the non-linear evolution of the natural frequency of the system during transient.
The resulting simple actuation and control strategy allows thus for a significant reduction of the loads transmitted through the mechanical structure during steady state operation. However, obtained simulation results show that deviating from the natural frequency of the system, translate into an increase in rod load. Furthermore, during start-up, the nominal load is still transmitted at 1 point of the run-up. Therefore, the next step consists in utilising the knowledge obtained from the transient behaviour to evaluate the possibility to minimise the reaction forces during start-up as-well.

Acknowledgement

Flanders Innovation & Entrepreneurship Agency (VLAIO) is gratefully acknowledged for its support within the Baekeland-mandate **HBC.2018.2055**. Furthermore, we acknowledge *Flanders Make* for the support of our team.

References

[1] R. Hartenberg and J. Danavit, *Kinematic synthesis of linkages*. New York: McGraw-Hill, 1964.

[2] K. Liang, R. Stone, W. Hancock, M. Dadd, and P. Bailey, "Comparison between a crank-drive reciprocating compressor and a novel oil-free linear compressor," *International Journal of Refrigeration*, vol. 45, 2014.

[3] P. Bailey, M. Dadd, and C. Stone, "An oil-free linear compressor for use with compact heat exchangers.," *International Conference on Compressors and their Systems*, pp. 259–268, 2009.

[4] S. Varedi, H. Daniali, M. Dardel, and A. Fathi, "Optimal dynamic design of a planar slider-crank mechanism with a joint clearance," *Mechanism and Machine Theory*, vol. 86, pp. 191 – 200, 2015.

[5] S. Yaqubi, M. Dardel, and H. M. Daniali, "Nonlinear dynamics and control of crank–slider mechanism with link flexibility and joint clearance," *Proceedings of the Institution of Mechanical Engineers, Part C: Journal of Mechanical Engineering Science*, vol. 230, no. 5, pp. 737–755, 2016.

[6] H.-S. Yan and W.-R. Chen, "On the output motion characteristics of variable input speed servo-controlled slider-crank mechanisms," *Mechanism and Machine Theory*, vol. 35, no. 4, pp. 541 – 561, 2000.

[7] H.-S. Yan and G.-J. Yan, "Integrated control and mechanism design for the variable input-speed servo four-bar linkages," *Mechatronics*, vol. 19, no. 2, pp. 274 – 285, 2009.

[8] H.-S. YAN and R.-C. SOONG, "An integrated design approach of four-bar linkages with variable input speed," *JSME International Journal Series C Mechanical Systems, Machine Elements and Manufacturing*, vol. 47, no. 1, pp. 350–362, 2004.

[9] X. Wang, Q. Ma, and Z. Zhu, "Low noise control of servo press," in *IECON 2007 - 33rd Annual Conference of the IEEE Industrial Electronics Society*, pp. 833–838, 2007.

[10] X. Wang, Q. Ma, and Z. Zhu, "Low noise control of servo press," in *IECON 2007 - 33rd Annual Conference of the IEEE Industrial Electronics Society*, pp. 833–838, 2007.

[11] J.-L. Ha, R.-F. Fung, K.-Y. Chen, and S.-C. Hsien, "Dynamic modeling and identification of a slider-crank mechanism," *Journal of Sound and Vibration*, vol. 289, no. 4, pp. 1019 – 1044, 2006.

[12] T. E. Shoup, "The design of an adjustable, three dimensional slider crank mechanism," *Mechanism and Machine Theory*, vol. 19, no. 1, pp. 107 – 111, 1984.

[13] F. J. Kay and R. E. Haws, "Adjustable Mechanisms for Exact Path Generation," *Journal of Engineering for Industry*, vol. 97, pp. 702–707, 05 1975.

[14] H. Zhou and K.-L. Ting, "Adjustable slider–crank linkages for multiple path generation," *Mechanism and Machine Theory*, vol. 37, no. 5, pp. 499 – 509, 2002.

[15] M. I. Sarigecili and I. D. Akcali, "Development of constant output–input force ratio in slider–crank mechanisms," *Inverse Problems in Science and Engineering*, vol. 27, pp. 565 – 588, 2019.

[16] R.-C. Soong, "A design approach for flexible linkage mechanisms with a rotational and a linear input," *Advanced Science Letters*, vol. 9, pp. 499–504, 04 2012.

[17] R.-C. Soong, "The new hybrid-driven mechanical presses," *Journal of Vibroengineering*, vol. 16, pp. 945–953, 2014.

[18] K. Liang, "A review of linear compressors for refrigeration," *International Journal of Refrigeration-revue Internationale Du Froid*, vol. 84, pp. 253–273, 2017.

[19] A. Beléndez, C. Pascual, D. Méndez, T. Beléndez, and C. Neipp, "Exact solution for the nonlinear pendulum," *Revista Brasileira de Ensino de Física*, vol. 29, pp. 645 – 648, 00 2007.

Appendix A. Derivation equation of motion

Starting from the kinetic and potential energy of the slider-crank system displayed in Fig. 1a, the following equations can be derived, where the kinetic energy can be written as a superposition of the linear movement of the piston and connecting rod as well as the rotation of the crank rod and tilting of the connecting rod.

$$\begin{aligned} T &= \frac{1}{2}I_r\dot{\theta}^2 + \frac{1}{2}I_l\dot{\phi}^2 + \frac{1}{2}m_p v_p^2 + \frac{1}{2}m_l v_l^2 \\ V &= m_r g\frac{r}{2}sin(\theta) + m_l g\frac{l}{2}sin(\phi) + \frac{k}{2}\Delta x^2 \end{aligned} \tag{A.1}$$

With

- $v_l = \sqrt{(\frac{dx_l}{dt})^2 + (\frac{dy_l}{dt})^2} = \sqrt{(rsin\theta + \frac{r^2 sin\theta cos\theta}{2\sqrt{l^2 - r^2 sin^2\theta}})^2 + (\frac{r}{2}cos\theta)^2}\dot{\theta}$
- $\dot{\phi} = \frac{rcos\theta}{l\sqrt{1-(\frac{r}{l}sin\theta)^2}}\dot{\theta}$
- $v_p = (-rsin\theta - \frac{r^2 sin\theta cos\theta}{\sqrt{l^2 - r^2 sin^2\theta}})\dot{\theta}$
- $\Delta x = rcos\theta + \sqrt{l^2 - r^2 sin^2\theta} - l$

Substituting the equalities above in the potential and kinetic energy formulations together with $lsin\phi = rsin\theta$ and denoting the recurring term $\sqrt{l^2 - r^2\ sin\theta^2}$ as a, the following equations are obtained:

$$\begin{aligned} a &= \sqrt{l^2 - r^2\ sin\theta^2} \\ \frac{da}{d\theta} &= -\frac{r^2 sin\theta cos\theta}{a} \end{aligned} \tag{A.2}$$

$$\begin{aligned} T = &\frac{1}{2}I_r\dot{\theta}^2 + \frac{1}{2}I_l\frac{r^2 cos^2\theta}{a^2}\dot{\theta}^2 + \frac{1}{2}m_p(-rsin\theta - \frac{r^2 sin\theta cos\theta}{a})^2\dot{\theta}^2 \\ &+ \frac{1}{2}((rsin\theta + \frac{\frac{1}{2}r^2 sin\theta cos\theta}{a})^2 + (\frac{r}{2}cos\theta)^2)\dot{\theta}^2 \end{aligned} \tag{A.3}$$

$$V = m_r\frac{r}{2}gsin\theta + m_l\frac{r}{2}gsin\theta + \frac{k}{2}(rcos\theta + a - l)^2$$

Deriving the Lagrangian L, with Q the non-conservative torques acting on the system:

$$\begin{aligned} L &= T - V \\ \frac{\mathrm{d}}{\mathrm{d}t}(\frac{\partial L}{\partial\dot{\theta}}) - \frac{\partial L}{\partial\theta} &= Q \end{aligned} \tag{A.4}$$

Starting with the derivation of the second term in the second equation of Eq. A.4:

$$\begin{aligned}\frac{\partial L}{\partial \theta} &= I_l\dot{\theta}^2\frac{r\cos\theta}{a}\frac{-r\sin\theta a-\frac{da}{d\theta}r\cos\theta}{a^2}\\ &+ m_p\dot{\theta}^2\left(r\sin\theta+\frac{r^2\sin\theta\cos\theta}{a}\right)\left(r\cos\theta+\frac{r^2\left(\cos^2\theta-\sin^2\theta\right)a-\frac{da}{d\theta}r^2\sin\theta\cos\theta}{a^2}\right)\\ &+ m_l\dot{\theta}^2\left(r\sin\theta+\frac{\frac{r^2}{2}\sin\theta\cos\theta}{a}\right)\left(r\cos\theta+\frac{1}{2}\frac{r^2\left(\cos^2\theta-\sin^2\theta\right)a-\frac{da}{d\theta}r^2\sin\theta\cos\theta}{a^2}\right)\\ &- m_l\dot{\theta}^2\left(\frac{r}{2}\cos\theta\right)\frac{r}{2}\sin\theta-(m_r+m_l)g\frac{r}{2}\ \cos\theta-k\ \ (r\cos\theta+a\ -l)\,(-r\sin\theta+\frac{da}{d\theta})\end{aligned} \tag{A.5}$$

Applying the chain rule on the first term of the second equation of Eq A.4:

$$\frac{d}{dt}\left(\frac{\partial L}{\partial\dot{\theta}}(\theta,\dot{\theta})\right)=\frac{\partial}{\partial\theta}\left(\frac{\partial L}{\partial\dot{\theta}}\right)\dot{\theta}+\frac{\partial}{\partial\dot{\theta}}\left(\frac{\partial L}{\partial\dot{\theta}}\right)\ddot{\theta} \tag{A.6}$$

$$
\begin{aligned}
\frac{\partial L}{\partial \dot{\theta}} = & \; I_r \; \dot{\theta} + I_l \frac{r^2 \cos^2\theta}{a^2}\dot{\theta} \; + m_p \left(-r\sin\theta - \frac{r^2 \sin\theta\cos\theta}{a} \right)^2 \dot{\theta} \\
& + m_l \left(\left(r\sin\theta + \frac{\frac{1}{2} r^2 \sin\theta\cos\theta}{a} \right)^2 + \left(\frac{r}{2}\cos\theta \right)^2 \right) \dot{\theta} \\
\frac{\partial}{\partial\theta}\left(\frac{\partial L}{\partial \dot{\theta}}\right)\dot{\theta} = & \; 2 I_l \dot{\theta}^2 \frac{r\cos\theta}{a} \frac{-r\sin\theta a - \frac{da}{d\theta} r\cos\theta}{a^2} \\
& + 2 m_p \dot{\theta}^2 \left(r\sin\theta + \frac{r^2\sin\theta\cos\theta}{a} \right) \left(r\cos\theta + \frac{r^2\left(\cos^2\theta - \sin^2\theta\right) a - \frac{da}{d\theta} r^2 \sin\theta\cos\theta}{a^2} \right) \\
& + 2 m_l \dot{\theta}^2 \left(r\sin\theta + \frac{\frac{r^2}{2}\sin\theta\cos\theta}{a} \right) \left(r\cos\theta + \frac{1}{2}\frac{r^2\left(\cos^2\theta - \sin^2\theta\right) a - \frac{da}{d\theta} r^2 \sin\theta\cos\theta}{a^2} \right) \\
& - 2 m_l \dot{\theta}^2 \left(\frac{r}{2}\cos\theta \right) \frac{r}{2}\sin\theta \\
\frac{\partial}{\partial\dot{\theta}}\left(\frac{\partial L}{\partial \dot{\theta}}\right)\ddot{\theta} = & \; I_r \; \ddot{\theta} + I_l \frac{r^2\cos^2\theta}{a^2}\ddot{\theta} + m_p \left(-r\sin\theta - \frac{r^2\sin\theta\cos\theta}{a} \right)^2 \ddot{\theta} \\
& + m_l \left(\left(r\sin\theta + \frac{\frac{1}{2} r^2 \sin\theta\cos\theta}{a} \right)^2 + \left(\frac{r}{2}\cos\theta \right)^2 \right) \ddot{\theta}
\end{aligned}
\tag{A.7}
$$

The final step consists in determining the non-conservative torques Q on the right hand side of Eq. A.4. The only non-conservative force considered in this investigation is the dissipating damping force proportional to the velocity of the piston (Fig. 1a and Table 1). To convert this damping force F_C into a counteracting torque T_C, the power balance is used:

$$
\begin{aligned}
F_C v_p &= T_c \dot{\theta} \\
-C v_p v_p &= T_c \dot{\theta}
\end{aligned}
\tag{A.8}
$$

As a result:

$$
\begin{aligned}
Q &= \frac{-C v_p^2}{\dot{\theta}} \\
&= -C \; (-r sin\theta - \frac{r^2 sin\theta cos\theta}{\sqrt{l^2 - r^2 sin^2\theta}})^2 \dot{\theta}
\end{aligned}
\tag{A.9}
$$

The resulting equation becomes:

$$
\begin{aligned}
I_r\ \ddot{\theta} &+ I_l \frac{r^2\cos^2\theta}{a^2}\ddot{\theta} + m_p\left(r\sin\theta + \frac{r^2\sin\theta\cos\theta}{a}\right)^2\ddot{\theta} \\
&+ m_l\left(\left(r\sin\theta + \frac{\frac{1}{2}r^2\sin\theta\cos\theta}{a}\right)^2 + \left(\frac{r}{2}\cos\theta\right)^2\right)\ddot{\theta} + I_l\dot{\theta}^2\frac{r\cos\theta}{a}\frac{-r\sin\theta a - \frac{da}{d\theta}r\cos\theta}{a^2} \\
&+ m_p\dot{\theta}^2\left(r\sin\theta + \frac{r^2\sin\theta\cos\theta}{a}\right)\left(r\cos\theta + \frac{r^2\left(\cos^2\theta - \sin^2\theta\right)a - \frac{da}{d\theta}r^2\sin\theta\cos\theta}{a^2}\right) \\
&+ m_l\dot{\theta}^2\left(r\sin\theta + \frac{\frac{r^2}{2}\sin\theta\cos\theta}{a}\right)\left(r\cos\theta + \frac{1}{2}\frac{r^2\left(\cos^2\theta - \sin^2\theta\right)a - \frac{da}{d\theta}r^2\sin\theta\cos\theta}{a^2}\right) \\
&- m_l\dot{\theta}^2\left(\frac{r}{2}\cos\theta\right)\frac{r}{2}\sin\theta + (m_r + m_l)g\frac{r}{2}\ \cos\theta + k\ \ (r\cos\theta + a\ - l)\left(-r\sin\theta + \frac{da}{d\theta}\right) = \ Q
\end{aligned}
\tag{A.10}
$$